

CONTINUED INVESTIGATION OF LDEF'S STRUCTURAL FRAME AND THERMAL BLANKETS BY THE METEOROID & DEBRIS SPECIAL INVESTIGATION GROUP

Thomas H. See
 Lockheed Engineering & Science Co.
 Houston, Texas 77058
 (713) 483-5027 / FAX (713) 483-5347

Kimberly S. Mack
 Lockheed Engineering & Science Co.
 Houston, Texas 77058
 (713) 244-5919 / FAX (713) 483-5347

Jack L. Warren
 Lockheed Engineering & Science Co.
 Houston, Texas 77058
 (713) 483-5122 / FAX (713) 483-5347

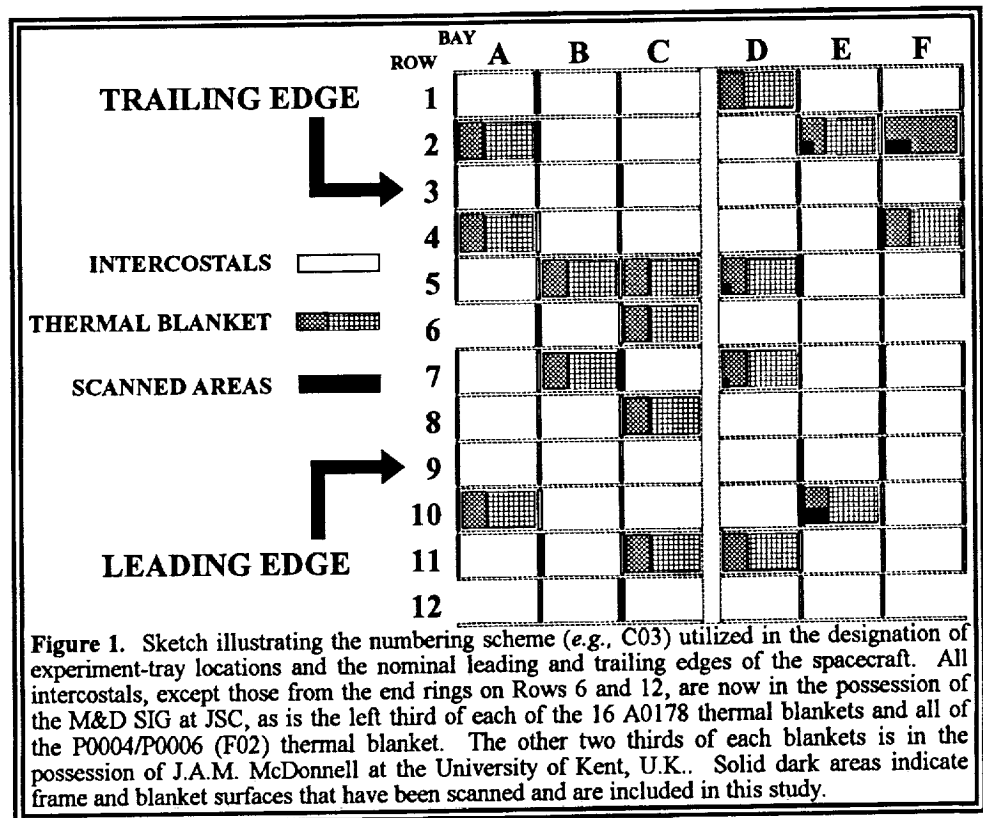
Michael E. Zolensky
 NASA / Johnson Space Center
 Houston, Texas 77058
 (713) 483-5128 / FAX (713) 483-5347

Herbert A. Zook
 NASA / Johnson Space Center
 Houston, Texas 77058
 (713) 483-5058 / FAX (713) 483-5276

INTRODUCTION

Since the return of the Long Duration Exposure Facility (LDEF) in January, 1990, the Meteoroid and Debris Special Investigation Group (M&D SIG) has been examining LDEF hardware (*i.e.*, experiment trays and structural components) in an effort to define the low-Earth orbit (LEO) particulate environment as witnessed by the spacecraft during its 5.7 year stay in orbit. Last year we reported (ref. 1) on the frequency of larger features as determined from data acquired by the M&D SIG's Analysis Team (A-Team) during LDEF deintegration. At that time the A-Team examined every square millimeter of the spacecraft locating and documenting the presence of all impact craters $\geq 500 \mu\text{m}$ in diameter and all penetration holes $\geq 300 \mu\text{m}$ in diameter (ref. 2). Over the past year M&D SIG members and Lockheed Engineering & Sciences Co. personnel at the Johnson Space Center (JSC) in Houston, Texas have been examining selected LDEF structural frame components (*i.e.*, intercostals) in much greater detail in order to augment this large-particle data with that from smaller particles.

In all, LDEF exposed



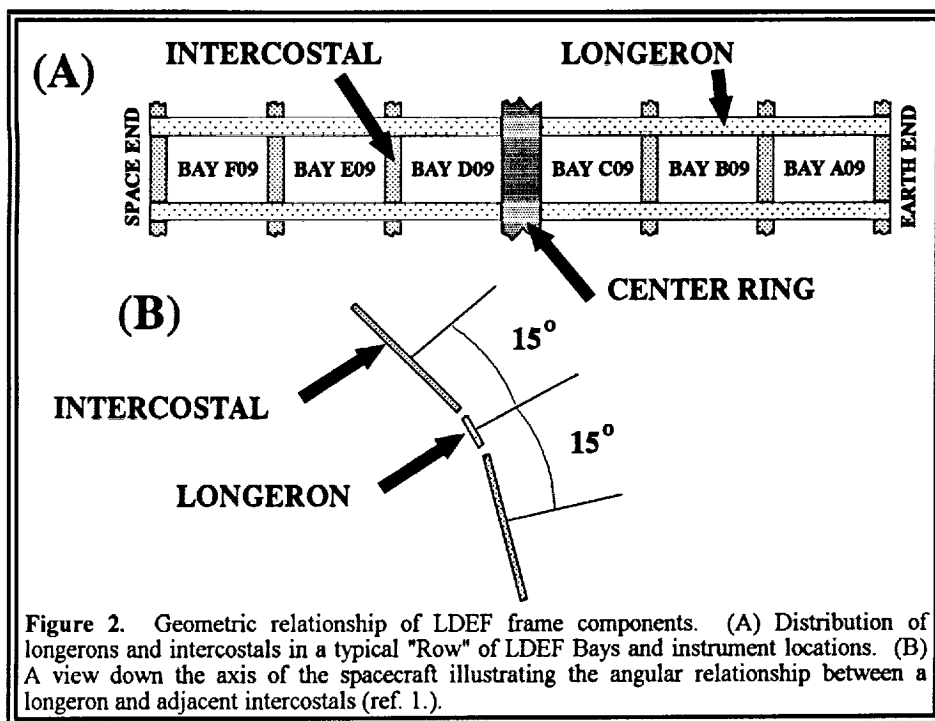
~130 m² of surface area to the LEO particulate environment, ~15.4 m² of which was occupied by structural frame components of the spacecraft. This report focuses on the data acquired by detailed examination of LDEF intercostals, 68 of which are now in possession of the M&D SIG at JSC (Figure 1). In addition, limited data will be presented for several small sections from A0178 thermal control blankets that were examined/counted prior to being shipped to Principal Investigators (PI's) for scientific study. As was the case in Ref. 1, the data presented here are limited to measurements of crater and penetration-hole diameters and their frequency of occurrence which permits, yet also constrains, more model-dependent, interpretative efforts. Such efforts will focus on the conversion of crater and penetration-hole sizes to projectile diameters (and masses), on absolute particle fluxes, and on the distribution of particle-encounter velocities. These are all complex issues (refs. 3, 4, 5, 6, 7, 8) that presently cannot be pursued without making various assumptions which relate, in part, to crater-scaling relationships, and to assumed trajectories of natural and man-made particle populations in LEO that control the initial impact conditions.

RATIONALE FOR SELECTION OF SURFACES

The size of a crater or penetration hole depends on the physical properties associated with the target and projectile materials, and on the projectile's mass and impact velocity. On LDEF, a given unit impactor generated craters of different sizes depending on the location or pointing direction of the target because of the different effective (mean) encounter velocity, assuming a constant target material. The quantitative relationships for these parameters are known for some LDEF materials, but only over a restricted range and set of initial conditions. In order for the M&D SIG to deduce particle frequencies as a function of directionality it is necessary to characterize impact features on identical target materials so that the physical

properties of the target can be accounted for, or remain constant. Furthermore, because of the highly stochastic nature of the collisional environment, it is also necessary to study materials which exposed sufficient surface areas to have accumulated a representative population of impact features. Such factors pointed to LDEF's structural frame as the *only* material that fit all of these criteria.

LDEF's entire structural frame was fabricated from 6061-T6 aluminum, a commonly used spacecraft material whose response to hyper-velocity impact has been

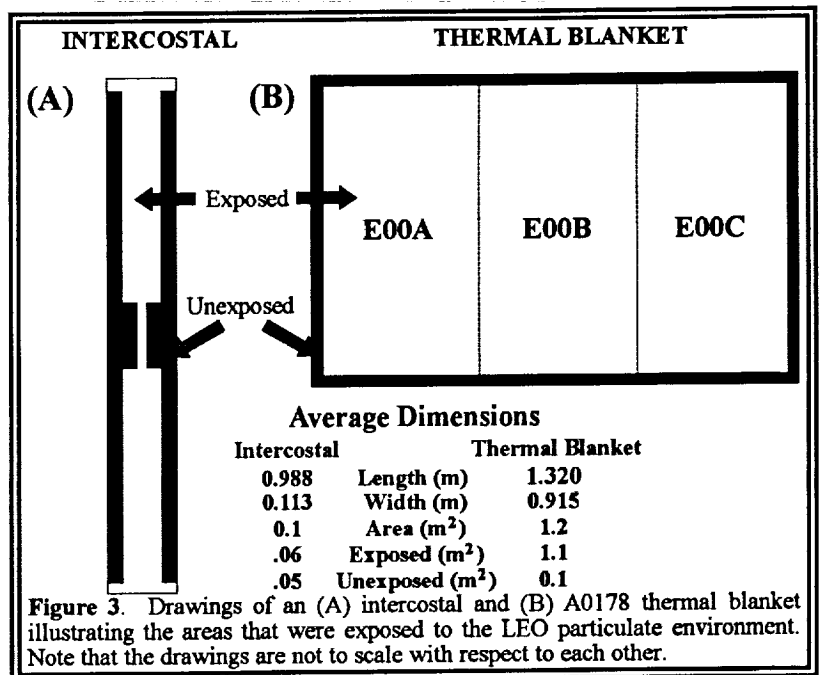


studied in great detail (e.g., refs. 3, 6, and 9). The frame components formed an open-grid, 12-sided structure that produced individual instrument bays (Bays A-F; Figure 1) and provided attachment points for the experiment trays. The longitudinal frame members (~4.6 m long) were termed "longerons" (Figure 2a), while cross members between longerons were called "intercostals" (~1 m in length). Individual rows were assigned sequential numbers (1-12), with Row 9 facing in the nominal velocity vector (leading-edge direction) and Row 3 in the trailing-edge direction. For simplicity, the M&D SIG assigned half-row numbers to the longerons (e.g., longeron 2.5 resides between Rows 2 and 3). The angle between adjacent instrument rows, defined by the intercostals, was 30° (resulting in the 12-sided cylindrical structure), while the angle between adjoining intercostals and longerons was 15° so that one longeron accommodated instruments from two adjacent rows (Figure 2b). The frame components of the Earth- and space-facing ends (i.e., Bays G and H) of the spacecraft were essentially flat. This configuration resulted in LDEF possessing 26 principal pointing directions (i.e., 24 around the periphery plus the Earth- and space-facing ends) and provides an unprecedented opportunity to study impact craters in a fairly well understood infinite halfspace target. Because of their size and mass, and because of their significance to the overall structural integrity of the spacecraft, the longerons and the components from the Earth- and space-facing ends could not be made available for detailed study in the laboratory. On the other hand, the small size and mass of the individual intercostals made them well suited for removal and detailed scanning within the Facility for the Optical Inspections of Large Surfaces (FOILS) laboratory at JSC.

Surface Areas and Procedures

Individual intercostals exposed ~0.06 m² of surface area (Figure 3a and Table 1), while a complete row of intercostals, not including the center ring (i.e., the four mid- and two end-ring intercostals; see Figures 1 and 2), totaled ~0.32 m²; end-ring intercostals exposed only ~0.04 m² each. Multiply by 12, and accounting for the two Row 6 and two Row 12 intercostals not included, results in a total exposed surface area of ~3.68 m² of LDEF intercostals in our study.

Although they were not as evenly distributed as the aluminum frame, the Scheldahl G411500 thermal blankets associated with the sixteen A0178 experiment trays and the one P0004/P0006 experiment tray offer another material type that was widespread around the exterior of LDEF (i.e., all rows except 3, 9 and 12 possessed at least one of these blankets; see Figure 1). Each blanket exposed ~1.1 m² (Figure 3b) of surface area and consisted of a 200 to 300 Å thick layer of silver-inconel that was sandwiched between a space-facing layer of FEP Teflon (~125 μm thick) and an 80 to 100 μm thick layer of DC1200 primer and Chemglaze Z306 black conductive paint. Unfortunately, the impact/penetration behavior of this composite foil is poorly understood at present and dedicated calibration experiments designed to address such behavior are needed.



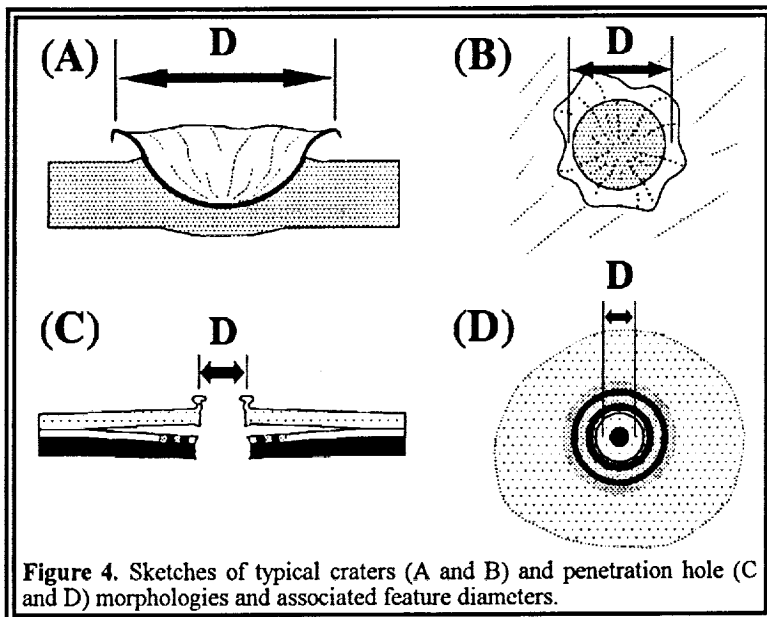


Figure 4. Sketches of typical craters (A and B) and penetration hole (C and D) morphologies and associated feature diameters.

As was the case in the earlier work (ref. 1) that utilized only the larger impact features on LDEF, crater diameters reported here for the intercostals refer to rim-crest-to-rim-crest dimensions (Figure 4a and 4b), while penetration-hole and crater diameters for the thermal blankets refer to center-of-rim-to-center-of-rim measurements (Figures 4c and 4d). For details on the morphology and associated measurement techniques for these, as well as all other impact features documented by the M&D SIG, interested readers should see Refs. 1 and 2. However, unlike the earlier effort, many of the features documented during the detailed examination of the thermal blankets were craters instead of penetration holes (see

below). In general, regardless of the feature size or event type, the outer layer (*i.e.*, the Teflon) still delaminated from the silver-inconel/thermal paint backing as illustrated in Figures 4c and 4d. Furthermore, most of these smaller impact features did not exhibit the associated rings that were so common with the larger penetration events into this same material (refs. 2 and 15).

Table 1. Number of individual features documented in each size bin for the LDEF intercostals and thermal blankets, as well as the associated exposed surface area for each component. Size bins are inclusive on the lower end of each bin (*i.e.*, bin 11 contains all particles $\geq 11 \mu\text{m}$ and $< 16 \mu\text{m}$ in diameter).

COMPONENT	INTERCOSTALS														TOTAL	SURFACE AREA (m ²)		
	<11	11	16	22	31	44	63	88	125	177	250	354	500	707			1000	1414
B01F02				2	1	4	7	7	3	5	2						31	0.0595
B02F02			5	4	2	7	10	10	1	1		1					41	0.0579
C03F02		1		4	5	3	4	3	5	1		1		1			30	0.0587
F04F02				1	1	3	4	3	1	2	1					1	18	0.0604
E05F02		10	38	14	14	5	7		2	3	2	1					96	0.0587
B06F02		2	10	17	10	11	3	5	3	2	1		1				65	0.0600
C07F02				9	28	34	45	11	19	16	8	5	4	1			180	0.0590
F07F02	40	63	143	148	42	49	16	15	10	7	3	3	2				501	0.0589
F08F02			4	4	40	25	33	19	17	9	6	6	3				167	0.0602
E09F02					28	22	52	20	18	12	6	2	4		1		165	0.0588
F09F02		10	32	80	65	77	29	36	22	15	7	4	5		2		384	0.0580
E10F02			19	18	65	38	39	18	14	17	11	1	8	1	2		251	0.0595
B11F02		1	10	15	9	42	23	26	12	8	6	3	1	1		1	158	0.0584
C12F02					1	7	19	12	7	7	4	1	1	1			60	0.0598
TOTAL	40	87	270	335	317	338	257	193	131	97	56	28	26	4	6	2	2147	

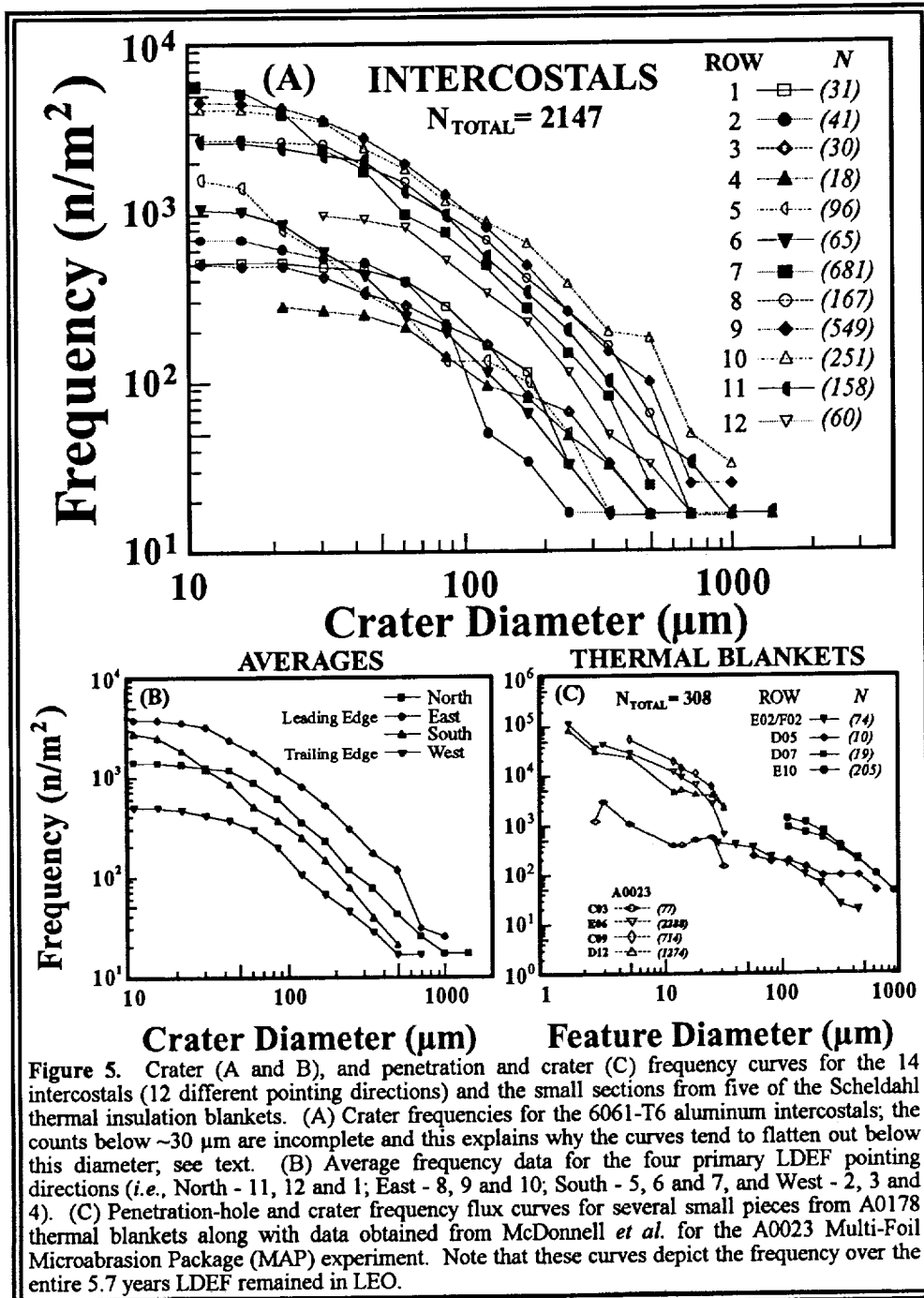
COMPONENT	THERMAL BLANKETS										TOTAL	SURFACE AREA (m ²)					
	10	14	20	28	40	57	80	113	160	226			320	453	640	905	1280
E02E00AA / F02E00AA			1	1	7	9	19	10	11	6	6	1	2	1		74	0.1615
D05E00AA							2		2	2				2		10	0.0411
D07E00AA								4	3	5	3	2	2			19	0.0212
E10E00AA / E10E00AC						2	1	29	60	55	26	17	8	5	2	205	0.1558
TOTAL			1	1	7	9	23	11	46	71	66	30	23	11	7	308	

Table 1 lists the number of features, sorted by size, documented on each LDEF row, as well as the exposed surface areas of each intercostal and thermal-blanket section that is included in the study. All scanning was conducted within the FOILS laboratory at JSC; the intercostals were scanned at a 40x magnification which easily permitted identification of all craters >30 μm in diameter on these relatively smooth surfaces. Thus, below 30 μm the coverage is not complete. During the scanning of the thermal blankets no attempt was made to document features <100 μm in diameter, except on components E02E00AA and F02E00AA which possessed a relatively small number of impacts to begin with and, therefore, were easily documented down to ~50 μm diameter features. It should be noted that no effort is

presently underway to conduct a systematic and comprehensive study of the thermal-blanket materials that are presently in the possession of the M&D SIG at JSC. The only thermal-blankets materials documented thus far at JSC are those that were being processed for shipment to various PI's for scientific study, some of which planned to totally consume the samples. Therefore, the statistics associated with these data are extremely poor and the data are presented here purely as supplementary information. It should be noted that McDonnell is examining sections of the other two thirds of these blankets.

RESULTS

The cumulative size frequency distribution and spatial density of craters and penetration holes are illustrated in Figure 5. Note that features ~200 μm in diameter in Figure 5C



generally occurred as craters and not penetration holes, because the increasingly smaller projectiles did not possess adequate size, mass and/or kinetic energy to completely penetrate the ~200 μm thick thermal blanket. In such cases the blanket responds as an infinite halfspace target resulting in a cratering instead of a penetration event.

Figure 5a displays the crater frequencies for the 14 intercostals examined to date (*i.e.*, one intercostal from each LDEF row except for Rows 7 and 9 on which two intercostals have been examined). These data are in good agreement with our earlier results (ref. 1) and with those of others (*e.g.*, ref. 11; not plotted for the sake of clarity), with the highest cratering rates being observed in the forward-facing directions (*i.e.*, Rows 8, 9 and 10) and the lowest frequencies found in association with the rearward-facing surfaces (*i.e.*, Rows 2, 3 and 4). In general, the slope for the various curves are very similar, suggesting overall ratios of large to small particles remaining relatively constant, regardless of pointing direction.

A possible exception to this relation can be seen in the curve associated with Row 7. Intercostal F07F02 possesses an unusually high density of craters <30 μm in diameter (see Table 1). Although no more effort was made to locate and document small features on this intercostal than any of the other 13 intercostals, the number of craters <30 μm in diameter is more than three times greater for F07F02 than for even the Row 9 leading-edge intercostals. In fact, F07F02 has 2.8 times more total craters, and more than 10 times the number of <30 μm diameter craters than does C07F02, an intercostal that was positioned on the opposite end of Row 2. Specifically, of the 681 craters documented on the two Row 7 intercostals, ~74% resided on F07F02, while 57% of the 681 craters were <30 μm in diameter and located on F07F02. Furthermore, the distribution of craters on F07F02 was evenly split between both ends of the intercostal, with 252 craters being located above the center clamp position (see Figure 3a), and 251 craters located below this central clamp position.

Several other surfaces on this same row and end of LDEF have exhibited a similar trend (Figures 5c and 6). At the request of the M&D SIG, Don Humes (personal communications, 1992) examined some of the hardware associated with the experiment trays located on either side of intercostal F07F02, since both bays were occupied by Humes' S0001 experiments. Figure 6 illustrates the results of Humes' investigation and depicts the results of his counts on an experiment-tray lip that resided on the F07F02 intercostal. The two Row 7 intercostals are plotted separately so that the unusual nature of the F07F02 intercostal is visible; also plotted are the frequency curves for the Row 9 and Row 3 intercostals. The Humes data exhibits an excellent match to our intercostal data between ~50 and 400 μm , and reveals an even higher flux below ~50 μm than does our data. The two intercostals from Row 7 are very different below ~30 μm , with intercostal

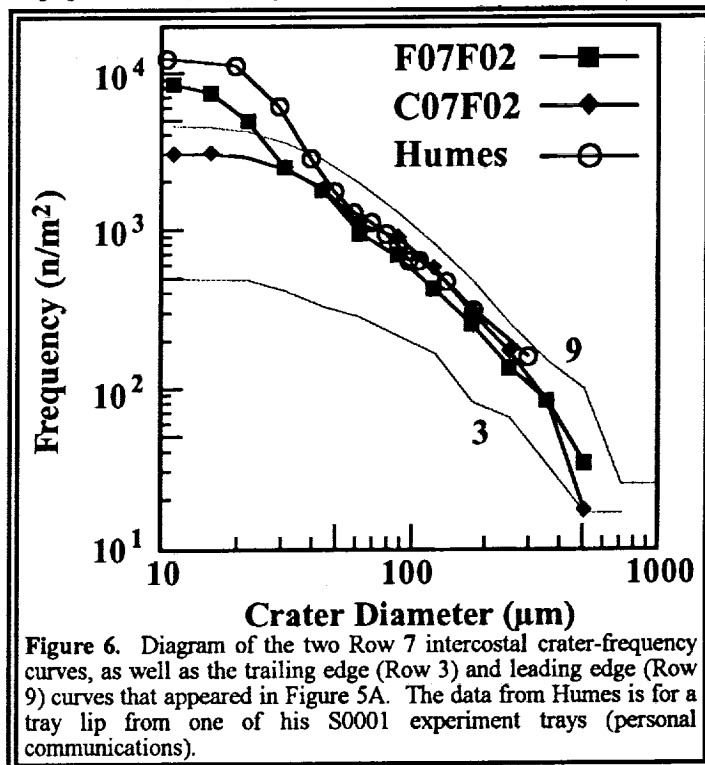


Figure 6. Diagram of the two Row 7 intercostal crater-frequency curves, as well as the trailing edge (Row 3) and leading edge (Row 9) curves that appeared in Figure 5A. The data from Humes is for a tray lip from one of his S0001 experiment trays (personal communications).

C07F02 displaying a trend that is similar to all other intercostals examined to date. An intercostal from Row 8 (F08F02) is included in this study, yet it does not exhibit the trend observed for F07F02.

There are two possible explanations for the variation of spatial densities of craters seen in the two separated locations on Row 7. The first possibility is that the variations are simply due to different

scanning biases from one location to another. The second and most likely possibility is that the observed variations do not suffer from observational biases and are of real statistical significance and need to be explained.

If the second possibility is true, then the variations must either be due to an extremely great variability in the spatial density of meteoroids or Earth-orbiting debris, or it is due to a source of impacting objects very near LDEF. The highest measured impact rate on LDEF was that by the Interplanetary Dust Experiment (IDE; ref. 7) where 131 impacts were recorded within an approximately two minute time period during LDEF's passage through a debris stream early in the mission. This corresponds to about one impact per second on the $\sim 1 \text{ m}^2$ IDE experiment. Since the orbital velocity of LDEF was $\sim 8 \text{ km/s}$, the spatial density of impacting objects -- even for this most intense stream -- did not exceed about $10^{-4}/\text{m}^3$, or about one impact per square meter per second. At such a rate no strong change in the integrated impacting flux at locations separated by several meters should be seen. As for sources very near LDEF, two possibilities come to mind. First, could all, or many of these small craters represent secondary craters? Potential locations of a primary crater have been explored, yet no potential source can be found. Nothing in the vicinity of this intercostal can be found that projects above the surface that could serve as a reasonable location for such a primary. The closest object protruding above the surface of the spacecraft is the Row 6 trunnion pin that was located on the center ring at a distance of more than two meters away and with a 30° angle between the rows. The other possible source might have been the nearby Space Shuttle during rendezvous maneuvers. This potential source can't yet be ruled out.

An alternative cause for the differences noted for Row 7 is some sort of optical scanning bias. We note, in Table 1, that nearly all the difference in crater spatial densities on Row 7 is due to craters smaller than $31 \mu\text{m}$ in diameter, meaning that most of these craters were smaller than are nominal scanning threshold of $30 \mu\text{m}$ (only above which are we confident of 100% coverage). It is not a question of statistics; the spatial density variations seen for craters less than $31 \mu\text{m}$ in diameter are clearly not due to Poisson statistical variations. Some sort of scanning bias -- not yet identified -- could cause the observed variations seen in Rows 7 and 9. We intend to scan selected areas from several intercostals and pointing directions at higher magnifications to help address the issue of possible scanning bias.

During the documentation of intercostal F07F02 it was noted that an unusually high number of these craters contained apparent residues. Therefore, after documentation of this intercostal was completed it was sectioned into 24 smaller pieces that could be examined in a Scanning Electron Microscope (SEM) in hopes of obtaining some qualitative chemical information regarding the projectile(s) responsible for these craters. To date, only 19 of the most promising craters, ranging in size from $10 \mu\text{m}$ to $95 \mu\text{m}$ in diameter, have been examined. Of these, four (21%) were found to contain residue of probable micrometeoritic compositions, three (16%) contained man-made (*i.e.*, two paint and one solder) material, two (11%) revealed chemistries that have commonly been associated with contamination on LDEF (*i.e.*, Si and Ca), and the remaining ten (53%) were indeterminate (*i.e.*, either insufficient amounts of residue were present or the resulting compositions could have more than one source). So far, these distributions appear like those observed for LDEF as a whole, and do not support a uniform particulate source for the abundant small craters identified on intercostal F07F02.

Obviously, the source(s) of these craters is (are) of extreme interest to the M&D SIG and further research into possible causes are under investigation. We presently plan on examining more of these features via optical and chemical techniques in hopes of providing more data to address this issue. The chemical distribution of those craters analyzed to date is most likely not representative of the entire intercostal since we purposefully chose craters that optically, at least, appeared to offer the best opportunities in providing chemical information.

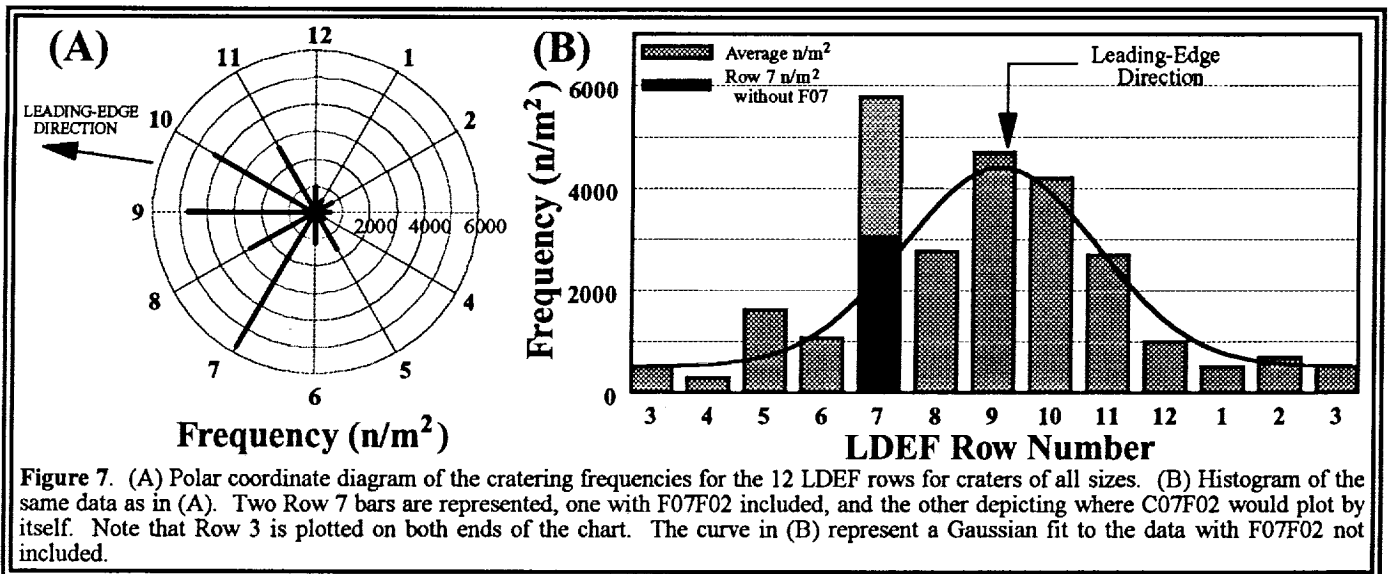


Figure 7. (A) Polar coordinate diagram of the cratering frequencies for the 12 LDEF rows for craters of all sizes. (B) Histogram of the same data as in (A). Two Row 7 bars are represented, one with F07F02 included, and the other depicting where C07F02 would plot by itself. Note that Row 3 is plotted on both ends of the chart. The curve in (B) represent a Gaussian fit to the data with F07F02 not included.

Returning to the general trends within our data, Figure 5b depicts the average frequencies for the four main LDEF pointing directions (*i.e.*, 12 [north], 9 [east], 6 [south] and 3 [west]). Each curve represents the average of the main row from each direction plus the rows on either side (*i.e.*, west represents the average of Rows 2, 3 and 4). Such a plot is useful in revealing the overall trends associated with each of these four pointing directions. As expected, the forward-facing rows reveal the highest cratering frequencies, while the rearward-facing rows exhibit the lowest. Also, not surprisingly, the northern facing rows (1, 12 and 11) display a slightly higher overall flux than do their southern-facing counterparts. Since LDEF's velocity vector was actually skewed $\sim 8^\circ$ toward Row 12 such a trend is understandable (*i.e.*, the northern-facing rows faced $\sim 8^\circ$ more into the velocity vector, while the southern-facing rows were $\sim 8^\circ$ further removed from the velocity vector, ref. 16; see Figure 7a). Again, note the influence of the F07F02 intercostal on the overall average flux associated with the southern-facing rows of Figure 5B.

Figure 7 depicts, in both polar and histogram form, the impact frequency for all sizes of craters (n/m^2) on each of the twelve rows. In our earlier efforts (refs. 1 and 13) that utilized only those craters $\geq 500 \mu m$ in diameter, we found that the highest cratering rates were associated with Row 10. However, now that we have greatly enhanced the data set and added much smaller features to our statistical database we find that the leading-edge or velocity vector did indeed experience the highest cratering rate (*e.g.*, ref. 12), again with the exception of the one Row 7 intercostal. The nearly 50% decrease in the large-cratering frequency for Row 9 versus Rows 8 and 10 that was discussed in Ref. 13 (see Figure 4 of ref. 13) disappears when much smaller craters are included (Figure 7a).

Figure 7b shows the same data plotted in histogram format and again illustrates the effect that intercostal F07F02 had on the average impact frequency for Row 7. The filled bar for Row 7 depicts where the Row 7 would fall if only the C07F02 intercostal was included. Finally, it can be seen that the intercostal data reveals a Gaussian-type distribution around the nominal leading-edge direction (Figure 7b). From a similar fit to the large-crater data in Ref. 13 we reported a leading-edge:trailing-edge ratio of $\sim 20:1$, while the Gaussian fit to the new intercostal data suggests a ratio more on the order of 10:1.

Figure 8a depicts the relative production rates for craters $\geq 44 \mu m$ and $\geq 63 \mu m$ in diameter and was generated by normalizing the absolute cratering frequencies for each row (Figure 7b) to that of Row 9 (leading-edge). At these crater sizes, there should be no biases introduced by incomplete scanning. This figure shows that the ratio of the production rate of impacts on the leading edge to that on the trailing edge is on the order of 10:1. Of equal interest is how this ratio varies as a function of crater size, an issue that is addressed in Figure 8b. For the larger craters (*i.e.*, $\geq 500 \mu m$ and $\geq 707 \mu m$ in diameter), Figure 8b indicates

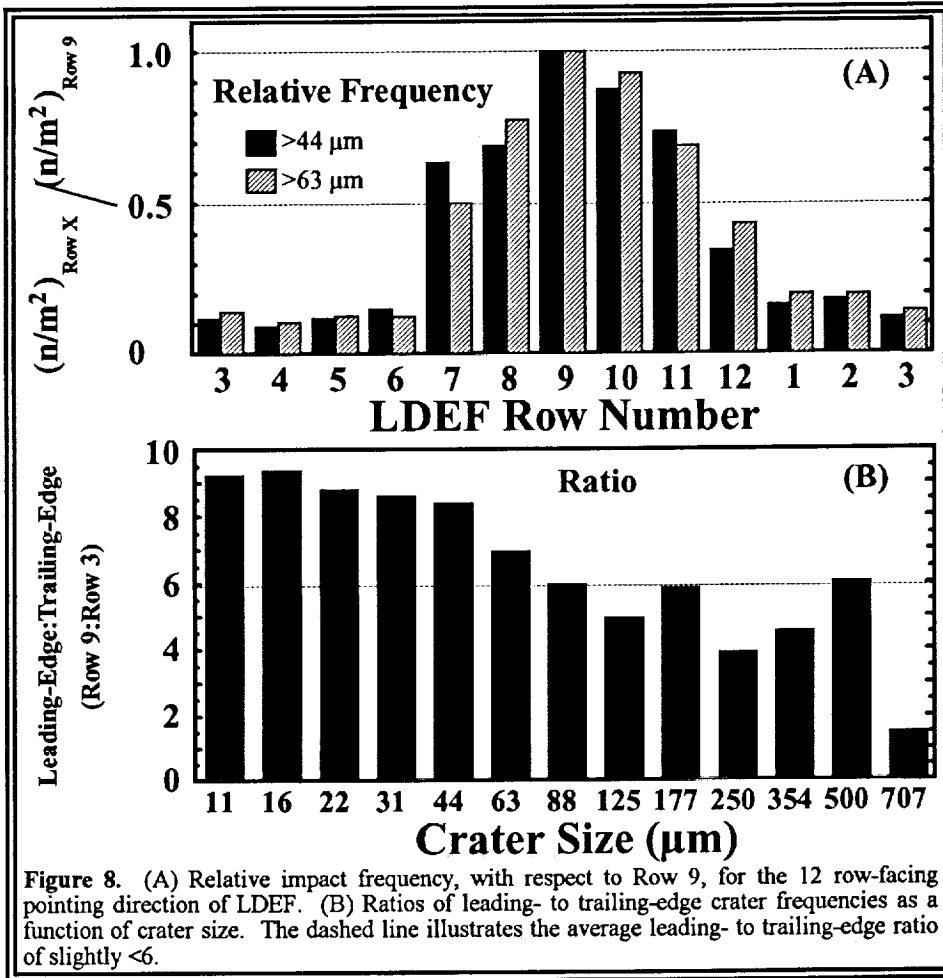


Figure 8. (A) Relative impact frequency, with respect to Row 9, for the 12 row-facing pointing direction of LDEF. (B) Ratios of leading- to trailing-edge crater frequencies as a function of crater size. The dashed line illustrates the average leading- to trailing-edge ratio of slightly <6.

a difference in the crater production rate between the leading- and trailing-edge of ~4 to 1, while for the smaller feature sizes this ratio is ~9:1. It should be noted that only 38 of the 2147 impacts (<2%) included in this study were $\geq 500 \mu\text{m}$ in diameter, resulting in a relatively large error associated with the 500 and 707 μm size bins. In general, however, there does appear to be a trend for the differences in feature production rate between the leading- and trailing-edge to increase as feature size decreases. Additional evidence for such a change can be found in the thermal-blanket and MAP experiment data illustrated in Figure 5c. For the larger penetration features (~500 μm in diameter) the leading- to trailing-edge ratio is ~10:1, while for the smallest features

for which data is available on both Rows 3 and 9 (*i.e.*, ~5 μm in diameter; see Figure 5c) this ratio climbs to ~50:1. Is the large-particle population more isotropically distributed, or are these difference related to the sources, and hence the associated velocities of the different particle-population sizes?

The measured ratios, Row 9 to Row 3, of the spatial density of impact craters do not agree with current theoretically predicted ratios for either meteoroids (ref. 12) or for Earth-orbital debris (ref. 14). Since it is believed that these two sources dominated all others on LDEF, it follows that the present theoretical models are inadequate to explain the data (ref. 17). For meteoroids to produce a front-to-back ratio as low as 6:1, a much larger fraction of high-velocity meteoroids than hitherto modeled seems to be required. If orbital debris is the primary source for the observed impact craters, the data suggest that there is much more debris than is now suspected in geosynchronous transfer orbits -- especially those with orbital inclinations near 28.5° (ref. 14). It may also be necessary to carefully reexamine the modeling for incorrect assumptions.

CONCLUSION

Last year we concluded that the observable impact record had to be expanded to include smaller impact features (ref. 1). Our current efforts are a step in that direction as we have continued to document various LDEF hardware (predominantly the structural frame) in order to better define and understand the LEO particulate environment. Our current results indicate that new theoretical modeling of both meteoroids and Earth-orbital debris needs to be undertaken. Specifically, new models should fit our latest observations of the directionality of crater spatial densities, and explore what these models imply in terms of sources of meteoroids or orbital debris.

Additional theoretical work is also needed to address other questions that have remained unanswered with respect to LDEF. What is the relationship between the sizes of the observed penetration holes in the Teflon thermal blankets with that of the observed crater sizes on the intercostals. Obviously, different materials pointing in the same general direction should have, overall, witnessed a similar particle population size over an extended period of time, such as the 5.7 years in which LDEF was in LEO. Questions such as these can only be addressed following a dedicated series of impact experiments into both of these materials. Such an effort will be a high priority of the M&D SIG over the next year. Is the observed 5.7 year average impact frequency representative of what is happening year after year, or is it simply an average of a highly variable particle population? Mullholland *et al.*, (ref. 7) present evidence that suggests the LEO particulate environment is quite dynamic and varies greatly as a function of time and orbital position. However, until additional data can be gathered such an idea remains controversial.

At present, we plan on continuing our scanning and documentation of the LDEF intercostals (at least until we have examined at least three intercostals per row) to improve our statistical database. In addition, it is hoped that the proposed calibration work for the thermal blankets can be conducted so that we can convert our cratering and penetration-hole frequencies into some sort of coherent particle-size population.

REFERENCES

- 1) See, T.H., Hörz, F., Zolensky, M.E., Allbrooks, M.K., Atkinson, D.R. and Simon, C.G., (1992) Meteoroid and Debris Special Investigation Group Preliminary Results: Size-Frequency Distribution and Spatial Density of Large Impact Features on LDEF. *LDEF - 69 Months in Space, First LDEF Post-Retrieval Symposium, NASA CP-3134*, p. 477-486.
- 2) See, T.H., Allbrooks, M.A., Atkinson, D.R., Simon, C.G. and Zolensky, M. (1990) *Meteoroid and Debris Impact Features Documented on the Long Duration Exposure Facility, A Preliminary Report, Publication #84, JSC #24608*, p. 583
- 3) Kessler, D.J. (1991) Orbital Debris Environment for Spacecraft in low Earth orbit, *J. Spacecraft*, 28, 3, p. 347-351.

- 4) Peterson, R.B. (1989) Instrument Pointing Considerations; *Report to Cosmic Dust Collection Facility Open Forum*, Lunar and Planetary Science Institute, March 1989
- 5) Zook, H.A. (1987) On cosmic dust trajectory measurements and experiment pointing considerations, in *Progress towards a Cosmic Dust Collection facility on Space Station*, Mackinnon, I.D. and Carey, W.C., eds., Lunar and Planetary Institute, LPI Technical Report 88-01, p. 76-77.
- 6) Zook, H.A. (1991) Meteoroid directionality on LDEF and asteroidal versus cometary sources (abstract). *Lunar Planet. Sci. XXII*, Lunar and Planetary Institute, Houston, Texas., p. 1577-1578.
- 7) Mullholland, J.D., Singer, S.F., Oliver, J.P., Weinberg, J.L., Cooke, W.J., Montague, N.L., Wortman, J.J., Kassel, P.C., and Kinard, W.H. (1992) IDE Spatio-Temporal Fluxes and High Time-Resolution Studies of Multi-Impact Events and Long-Lived Debris Clouds. *LDEF - 69 Months in Space, First LDEF Post-Retrieval Symposium, NASA CP-3134*, p. 517-528.
- 8) Hörz, F., Messenger, S., Bernhard, R., See, T.H. and Haynes, G. (1991) Penetration phenomena in Teflon and aluminum films using 50-3200 μ m glass projectiles (abstracts), *Lunar Planet. Sci. XXII*, Lunar and Planetary Institute, p. 591-592.
- 9) Cour-Palais, B.G. (1987) Hypervelocity Impacts in Metals, Glass, and Composites, *Int. J. Impact Eng.*, 5, p. 681-692.
- 10) McDonnell, J.A.M. and Stevenson, T.J. (1992) Hypervelocity Impact Microfoil Perforations in the LEO Space Environment (LDEF, MAP A0023 Experiment). *LDEF - 69 Months in Space, First LDEF Post-Retrieval Symposium, NASA CP-3134*, p. 443-458.
- 11) Hörz, F., Bernhard, R.P., Warren, J.L., See, T.H., Brownlee, D.E., Laurance, M.R., Messenger, S. and Peterson, R.B. (1992) Preliminary Analysis of LDEF Instrument A0187-1 "Chemistry of Micrometeoroids Experiment." *LDEF - 69 Months in Space, First LDEF Post-Retrieval Symposium, NASA CP-3134*, p. 487-502.
- 12) Zook, H.A., (1992) Deriving the Velocity Distribution of Meteoroids From the Measured Meteoroid Impact Directionality on the Various LDEF Surfaces. *LDEF - 69 Months in Space, First LDEF Post-Retrieval Symposium, NASA CP-3134*, p. 569-579.
- 13) Zolensky, M., Atkinson, D., See, T.H., Allbrooks, M., Simon, C., Finckenor, and Warren, J. (1991) Meteoroid and Orbital Debris Record of the Long Duration Exposure Facility's Frame, *J. Spacecraft and Rockets*, 28, #2, p. 204-209.
- 14) Kessler, D.J., Origin of Orbital Debris Impacts on LDEF's Trailing Surfaces. *LDEF - 69 Months in Space, Second LDEF Post-Retrieval Symposium, NASA CP-3194, 1993*.
- 15) Allbrooks, M. and Atkinson, D. (1992) *The Magnitude of Impact Damage on LDEF Materials*. A final report to the M&D SIG under subcontract NAS9-17900, SC-02N0165768 to Lockheed - ESC.

- 16) Peters, P.N. and Gregory, J.C. (199) Attitude Stability of LDEF: Refinement of Results from the Silver Pinhole Camera. *LDEF - 69 Months in Space, Second LDEF Post-Retrieval Symposium, NASA CP- NASA CP-3194, 1993.*
- 17) Coombs, C., Watts, A., Wagner, J. and Atkinson, D. (1992) *LDEF Data: Comparisons with Existing Models.* A final report to the M&D SIG under subcontract NAS9-17900, SC-02N0165768 to Lockheed - ESC.